Artificial cathode electrolyte interphase by functional additives toward long-life sodium-ion batteries

Iqra Moeez [a], Dieky Susanto [a], Wonyoung Chang [a,b], Hee-Dae Lim [a,b,*], Kyung Yoon Chung [a,b,*]

[a] Center for Energy Storage Research, Korea Institute of Science and Technology, Hwarangro 14-gil 5, Seongbuk-gu, Seoul 136-791, Republic of Korea
[b] Division of Energy & Environment Technology, KIST School, Korea University of Science and Technology, Seoul 02792, Republic of Korea

ARTICLE INFO

ABSTRACT

Although $Na_{0.67}Fe_{0.5}Mn_{0.5}O_2$ has attracted tremendous attentions as a cathode material for sodium-ion batteries (NIBs), undesirable side reactions at the interphase between the electrode and electrolyte have limited its wide utilization. An effective way to prevent the side reaction is to artificially induce a mechanically robust and chemically stable cathode electrolyte interphase (CEI). In this paper, functional additives of NaF and Na_2CO_3 were used to artificially form a thick and stable CEI layer, and their effects were deeply investigated. It was demonstrated that the functional additives in electrolytes could be partially decomposed during a charge process, then it could play a key role in forming a thick and stable interphase directly on the cathode surface. The newly formed CEI layer could sup- press the dissolution of transition metals into the electrolyte and prevent the deterioration of the solid interphase layer. As a result, the additives successfully prevent the capacity fading problem of $Na_{0.67}Fe_{0.5}Mn_{0.5}O_2$ during electrochemical cycling, which results in the improved cyclability compared to the bare $Na_{0.67}Fe_{0.5}Mn_{0.5}O_2$. We believe that the addition of functional additive is a simple and cost-effective way to artificially form a stable CEI layer on a cathode, therefore, this approach is expected to be widely applicable to other electrode materials that suffer from the unstable interfaces.

1. Introduction

The rapid market development of electronic devices have naturally forced current lithium-ion batteries (LIBs) to advance to next-generation energy storage systems [1–4]. To successfully progress into next-generation batteries, essential requirements such as a low cost, long service life, and high energy efficiency should be satisfied by electrode materials for the future batteries. Currently, sodium-ion batteries (NIBs) have been increasingly studied as an ideal alternative system to LIBs owing to the natural abundance of sodium, which is much cheaper and environmentally friendly compared to lithium [3–8]. Naturally, many efforts have been made to develop appropriate electrode materials for NIBs, which can provide better performances beyond that of current LIBs. Among them, layered metal oxides ($NaMO_x$), especially Mn-based layered oxides, have been actively researched because they have great potential to meet the requirements of high energy efficiency even with a low cost [1,9–11]. As a representative active material, P2-type $Na_{0.67}Fe_{0.5}Mn_{0.5}O_2$ (NFMO) has been developed as a promising cath-ode due to its high theoretical capacity (260 mAh g^{-1}) as well as the relatively high operating voltage [12–14]. These materials with P2-type layered structures show relatively reversible sodiation/de-sodiation re-actions when they operate below 4.0 V. However, once charged over 4.0 V, they degrade quickly with the large irreversible capacity losses due to the irreversible structural changes. Particularly, P2 phase undergo a series of slab gliding processes during the sodium extraction process. In addition, phase transition from P2 to O2 could be triggered if Na is over-extracted from the host structure, implying the structural instability of P2-type layered oxides at a deep-charged state (up to 4.3 V) [15,16]. Besides structure instability at high voltage, decomposition of electro-lyte also initiates degradation of the electrodes. As, these decomposed products start to accumulate at the interphase and get involved in the side reactions with active species in cathodes, such as the transition metal ions (e.g., Mn) and oxygen anions, leading to capacity fade and limiting its practical application [17–19]. Also, the degradation of a salt (e.g., sodium hexafluorophosphate, $NaPF_6$) or an additive (e.g., fluoro-ethylene carbonate, FEC) in the electrolyte at a high voltage near 4.3 V has been a problematic issue because they produce hazardous byprod-ucts such as pentafluoride (PF_5) and hydrofluoric acid (HF), eventually leading to cell failure [20–26].

As an effective approach to solve these prevailing problems, the

---

formation of a stable cathode electrolyte interphase (CEI) layer directly on the cathode material has been suggested [23,27–35]. CEI is a chemically formed layer at the interface between electrode and electrolyte from the reduction of the electrolyte, and it is mainly composed of organic species (*e.g.,* –CH, –CO, and -CF) and inorganic species (*e.g.,* Na_2CO_3, Na_2CO_3R, NaCl, and NaF) [32,36,37]. Normally, various organic species are formed in CEI mostly near the electrolyte side, while inorganic species are located relatively close to the electrode surface [32,37,38]. Importantly, Na_2CO_3 and NaF are demonstrated to be key components that serve to produce a robust and stable CEI layer, which not only prevents side reactions with the electrolyte but also contributes to a fast charge transfer [32,37]. However, intentionally incorporating these two ideal components as major components in the CEI layer has been rarely achieved because the formation of CEI is spontaneous chemical reaction and difficult to control. Moreover, the CEI layer is sensitively dependent on the applied potentials during cell operations and is prone to be dissolved or deformed at high voltages [38]. If the protecting CEI layer collapses, the newly exposed surface triggers undesirable side reactions such as electrolyte decomposition, the formation of transition metal fluorides, and the loss of active material, finally leading to the cell degradation [9,21,30,38]. If the original CEI could be tuned into the artificial layer by mostly composing Na_2CO_3 and NaF, it must be an effective strategy for improving the energy efficiency of NIBs as well as providing a long cycling life.

In this paper, to artificially induce a stable and thick CEI layer on an NFMO cathode, Na_2CO_3 and NaF, as functional additives, were directly dissolved in an electrolyte prior to electrochemical cycling. It is demonstrated that these additives could be decomposed during the charging process and formed a thicker CEI layer on the NFMO cathode that mostly consisted of Na_2CO_3 and NaF. This simple modification could effectively alleviate the dissolution of transition metals, resulting in an improved electrochemical performance. Various analyses, such as X-ray absorption spectroscopy (XAS), X-ray photoelectron spectroscopy (XPS), and time-of-flight secondary ion mass spectrometry (TOF-SIMS), were used to closely investigate the role of additives, and we revealed that the structural and compositional changes in the artificial CEI layer could attribute to the improved cycling performance of the promising NFMO cathode.

2. Results and discussion

The schematic diagram shown in Fig. 1 describes our strategy to induce a stable CEI through the simple addition of functional additives in the electrolyte. Most cathode materials used for NIBs naturally contain thin CEI layers at their interfaces by contacting with the electrolyte, and these CEI layers are composed of complex mixtures of organic and inorganic species (*e.g.,* –CH, –CO, and -CF and Na_2CO_3, Na_2CO_3R, NaCl, and NaF, respectively) [32,37]. Unfortunately, these CEIs are relatively thin and unstable (Fig. 1a), and easy to dissolve or decompose at high voltages [32,37,38]. Then, the exposure of active material to the electrolyte initiates continuous side reactions, resulting in a decreased energy efficiency. To prevent cycle degradation, we artificially induced a thick and stable CEI layer by using Na_2CO_3 and NaF as functional additives (Fig. 1b). These two components are well known to improve the mechanical strength of a CEI layer and provide good adhesion, thereby it is expected to help forming a stable and thick CEI that effectively suppresses the undesirable side reactions [32,37]. In this respect, we simply added Na_2CO_3 and NaF additives to the electrolyte and electrochemically decomposed them during the first charging process, which enabled them to be intentionally incorporated into the pristine CEI layer. If they could form a dense layer mainly consisting of Na_2CO_3 or NaF-related compounds, the tuned CEI layer is expected to prevent the side reactions and improve electrochemical performance.

To demonstrate the effect of functional additives (Na_2CO_3 and NaF), electrochemical performances were investigated according to the presence or absence of the treatment, as shown in Fig. 2. The cathode material of NFMO was prepared by using a solid-state method [12], and powder X-ray diffraction (XRD) confirmed that NFMO with a $P6_3/mmc$-layered structure was well synthesized without any impurities (Fig. S1). A reference electrolyte of 1 M $NaClO_4$ in propylene carbonate (PC): fluoroethylene carbonate (FEC) (98: 2 by wt. %) was used, and 2% of each Na_2CO_3 and NaF (based on the total weight of $NaClO_4$) was added to this electrolyte. It has been reported that the deintercalation of sodium ions during the charging process is associated with the oxidation of Mn^{+3} to Mn^{+4} (<3.8 V) followed by the oxidation of Fe^{+3} to Fe^{+4} (>3.8 V) [12,16]. Accordingly, the cutoff voltages were limited to a range of 1.5 to 4.3 V (*vs.* Na/Na^+) to fully utilize the Mn^{+3}/Mn^{+4} and Fe^{+3}/Fe^{+4} redox reactions. As shown in the first cycle (Fig. 2a), bare NFMO without additives (*i.e.*, NFMO-w/o additives) shows a discharge

Fig. 1. Schematic illustration showing the different formations of CEI layers on the $Na_{0.67}Fe_{0.5}Mn_{0.5}O_2$ (NFMO) electrode surfaces. Images of the original CEI layer formed (a) without additives (NFMO-w/o additives) and the modified CEI by (b) Na_2CO_3 and NaF additive.
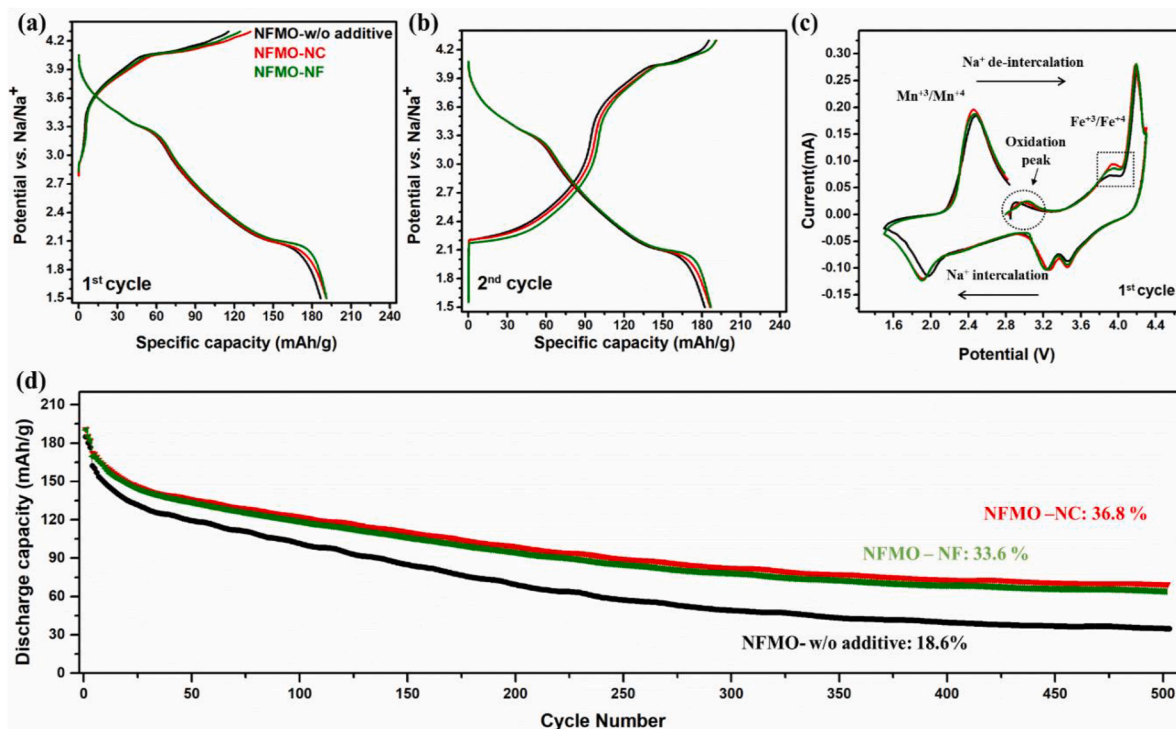
Fig. 2. Galvanostatic charge and discharge profiles in (a) the first and (b) second cycle of NFMO electrodes without additive (NFMO-w/o additives), and with Na_2CO_3 (NFMO-NC) and NaF (NFMO-NF) additives. Comparisons of (c) CV curves measured at 0.1 mV s^{-1} and (d) long-term cycling performances at a constant rate of 0.5C.

capacity of 186 mAh g^{-1}, while NFMO electrodes with electrolytes containing 2% Na_2CO_3 and NaF (described as NFMO-NC and NFMO-NF, respectively) show slightly higher discharge capacities. NFMO-NC and NFMO-NF deliver discharge capacities of 197 and 196 mAh g^{-1}, respectively, by presenting a slightly longer plateau near 2.0 V. Notably, these increased capacities can be maintained in the subsequent cycles (Fig. 2b). The charge capacities at the second cycle for both NFMO-NC and NFMO-NF are close to 192 mAh g^{-1}, and both values are slightly higher to that of NFMO-w/o additives (182 mAh g^{-1}). In short, the addition of additives can enhance the reversible capacity of the NFMO electrode, and the improvement may be attributed to the formation of an artificial CEI layer. Detailed analyses of the modified CEI layer will be discussed later.

To closely investigate the effects of the additives on the electrochemical profiles, CV was conducted for NFMO-w/o additives, NFMO-NC, and NFMO-NF (Fig. 2c). The CV curves of the NFMO-w/o additives (black line) show reversible Mn^{+3}/Mn^{+4} and Fe^{+3}/Fe^{+4} redox peaks at approximately 2.4/2.1 and 3.9/3.2 V, respectively, indicating the de-intercalation/intercalation of sodium ions. The redox peaks at 4.2/3.5 V correspond to the phase transition of a P2-type NFMO to an O2-type disordered phase [15,39]. In the initial anodic scans of NFMO-NC and NFMO-NF, distinct oxidation peaks at 3.0 V (in the dotted circle) are observed due to the oxidation of functional additives Na_2CO_3 and NaF. The small oxidations were also observed in the previous reports similarly using the additives [34,40]. This electrochemical oxidation plays a crucial role for modifying CEI layer by inducing compositional and structural changes. Importantly, the oxidation peak for the Fe^{+3}/Fe^{+4} redox reactions in NFMO-NC and NFMO-NF shows a noticeable increase (in the dotted square box) compared to NFMO-w/o additives; furthermore, NFMO-NC and NFMO-NF show a more intense reduction peak of Mn^{+3}/Mn^{+4} at potentials between 1.8 and 2.2 V. The increased intensities of the Mn and Fe redox peaks explain the reason for the slightly increased capacities demonstrated in Fig. 2a and b. This result suggests that the modified CEI layer can protect the active material from side reactions and suppress the dissolution of active materials.

Additionally, the effect of each additive on the long-term cycling performance is investigated, as shown in Fig. 2d. In regard to NFMO-w/o additives, the initial discharge capacity of 186 mAh g^{-1} gradually decreases after cycling, and the capacity retention after 500 cycles is only approximately 18.6%. On the other hand, the presence of functional additives in the electrolyte can increase the capacity retention of NFMO-NC and NFMO-NF to 36.8% and 33.6%, respectively, after 500 cycles. Additional electrochemical analyses of electrochemical impedance spectroscopy (EIS) and rate capability test were investigated. EIS (Fig. S2) results clearly show that charge transfer resistances of NFMO-NC and NFMO-NF are far lower than that of the NFMO-w/o additives. As a result, rate capabilities (Fig. S3) in the presence of functional additives were also improved compared to the NFMO-w/o additives. Considering that cycle degradation is mainly responsible to the side reactions, such as the accumulation of electrolyte decomposition products and the dissolution of transition metals [21,22,41,42], additives are expected to suppress these undesirable reactions.

To investigate the properties of tuned CEI layers in the presences of functional additives, we performed soft XAS measurements (Fig. 3) at the Na K-edge, O K-edge, F K-edge, and C K-edge. Pristine NFMO corresponds to the bare electrode before cycling (dotted line), while NFMO-w/o additives, NFMO-NC, and NFMO-NF (solid lines) describe electrodes after one cycle (*i.e.*, after the first charge and discharge). The total electron yield (TEY) absorption spectra of the C K-edge for pristine NFMO (dotted line in Fig. 3a) show three distinct peaks at 285.4, 288.3, and 290 eV. The peak at 285.4 eV corresponds to the single-bond π states of C—C bonds from amorphous carbon, and the peak at 288.3 eV is due to $-CH_2$ elements from the electrolyte and polyvinylidene fluoride (PVDF) binder [43–45]. Their overall intensities in pristine NFMO were decreased compared to the one-cycle electrodes (NFMO- w/o additives, NFMO-NC, and NFMO-NF). It is because the bare surface of NFMO was covered by the CEI layer after the electrochemical charge and discharge processes. It should be noted that the peak of Na_2CO_3 (290 eV) becomes much more intense in the cases of NFMO-NC and NFMO-NF (red line and green line, respectively) compared to that of NFMO-w/o additives (black
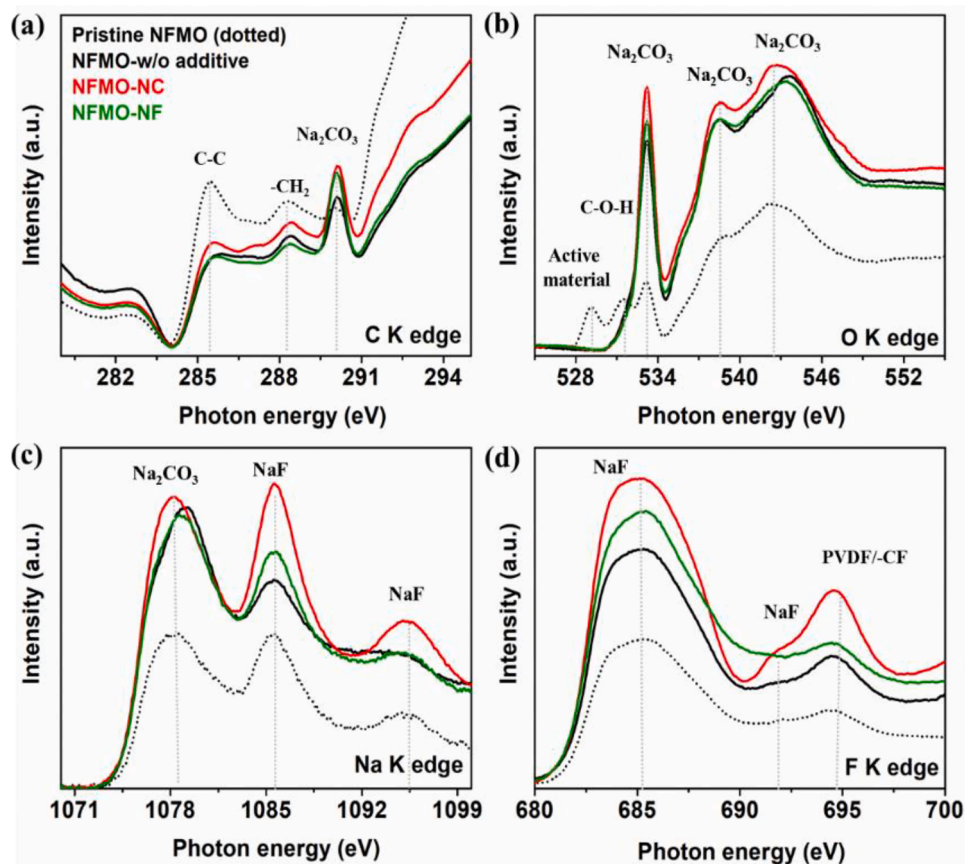
Fig. 3. Characterization of the CEI layer by using XAS. Absorption spectra of pristine NFMO and one-cycle NFMO electrodes (*i.e.,* NFMO-w/o additives, NFMO-NC, and NFMO-NF after completing the first charge and discharge) were obtained: (a) C K-edge, (b) O K-edge, (c) Na K-edge, and (d) F K-edge.

line), which demonstrates that the additives are surely effective in changing the CEI compositions.

Compositional changes are also observed in the TEY absorption spectra of the O K-edge and Na K-edge. In the O K-edge spectra (Fig. 3b), the peak at 529 eV is responsible for metal oxides (Fe−O and Mn-O) from the active material, and the peak at 531.5 eV is from the C−O−H bonds in the PVDF binder [43,44]. These peaks disappear for the one-cycle electrodes, again suggesting the formation of CEI layer on the electrode surface. Notably, the peaks of Na_2CO_3 at 533.3, 538.5, and 542 eV [45] are much more intense in the case of one-cycle electrodes compared to those of pristine NFMO, which is similarly observed in Fig. 3a. Additionally, it is worth mentioning that the Na_2CO_3 peak is mostly dominant in the case of NFMO-NC (red line), where the Na_2CO_3 additive is directly added to the electrolyte. In the TEY signal at the Na K-edge (Fig. 3c), pristine NFMO exhibits two peaks of Na_2CO_3 (1079 eV) and NaF (1085.5 eV), and their peak intensities are increased after the one-cycle due to the formation of CEI layer. Also, it is reasonable that the peak intensity of NaF (1085.5 eV) for NFMO-NF is higher than that of NFMO-w/o additives considering that NFMO-NF is a pre-treated one with NaF additive before cycling. Even in the case of NFMO-NC, where the Na_2CO_3 additive is used in the absence of NaF, a high content of NaF in the CEI layer is unexpectedly detected. It is because HF from the decomposition of FEC at a high voltage [24] reacted with carbonate compounds in the CEI layer [46] and produced NaF. The presence of NaF in NFMO-NC is also observed in the TEY spectra at the F K-edge (Fig. 3d). Fig. 3d shows that the intensities of NaF peaks (685.0 eV) increase with the addition of additives (NFMO-NC and NFMO-NF) compared to NFMO-w/o additives. The peak at 694 eV is especially dominant for NFMO-NC because it overlaps with the signal from the -CF organic species, whose amount can increase due to the Na_2CO_3 additive reacting

with FEC [32,43,46]. In short, the XAS analyses reveal two conclusions: (1) the formation and coverage of CEI layer on the electrode surface after electrochemical cycling and (2) the contents of Na_2CO_3 and NaF in the CEI compositions increase in NFMO-NC and NFMO-NF compared to NFMO-w/o additives. In other words, it is demonstrated that the additives enable to induce compositional changes in the CEI layer.

To closely analyze the surface characteristics of the tuned CEI layer, XPS was conducted (Fig. 4a–c). XPS spectra for the pristine NFMO electrode exhibit the typical peaks related to the active material, amorphous carbon black, PVDF binder, NaF, Na_2CO_3, C−O, and C=O species on the electrode surface [38]. Notably, all the one-cycle electrodes show the additional peaks of carbonates (Na_2CO_3 and $RNaCO_3$) as described by the blue region in the C 1 s spectra (Fig. 4a). This result well supports the above two conclusions from the XAS results. Moreover, as shown in O 1 s (Fig. 4b), the dominant peak of the active material (orange region) observed with pristine NFMO is greatly reduced in the spectra of the one-cycle electrodes; instead, relatively higher intensities for Na_2CO_3 (gray region) are observed. This phenomenon is more dominant in the cases of NFMO-NC and NFMO-NF, demonstrating that the additives effectively form a thick CEI layer accompanied by compositional changes. The formation of the CEI layer is also observed in the F 1 s XPS spectra (Fig. 4c). The peak intensity of PVDF in pristine NFMO (688 eV, orange region) is decreased in one-cycle electrodes. Furthermore, a relatively higher peak at 688 eV for NFMO-NC is attributed to the -CF compounds, as we described in Fig. 3d. It is worth noting that the green and blue regions, corresponding to the transition metal fluorides (MnF and FeF, respectively) in NFMO-w/o additives, decrease for NFMO-NC and NFMO-NF. This result suggests that the metal fluorides, whose presence indicates the problematic metal disso-lutions, can be somewhat suppressed by the use of additives, which
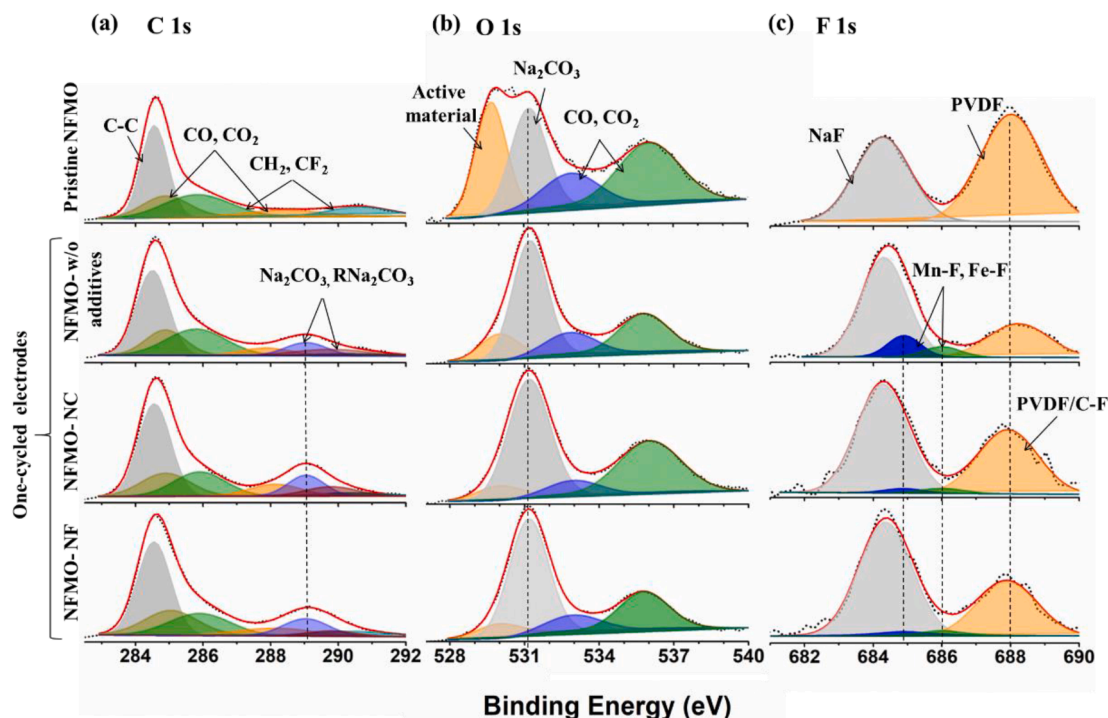
Fig. 4. Comparison of the (a) C 1 s, (b) O 1 s, and (c) F 1 s XPS spectra of pristine NFMO and the one cycle electrodes. The dotted (black) and solid (red) spectra present the observed spectra and the summation of peak energies, respectively.

should be a reason for the improved electrochemical performances shown in Fig. 2. Additionally, to investigate whether the compositional changes of CEI layers were actually induced by the initial charge process, XPS results for the electrodes after the first charge to 3.2 V were analyzed in Fig. S4.

For a further compositional analysis on the electrode surface, time-of-flight secondary-ion mass spectrometry (TOF-SIMS) was used because it provides ultrahigh chemical selectivity and sub nanometer surface sensitivity [21]. A series of TOF-SIMS depth profiles (Fig. 5a and b) present the compositional depth-profile information on the CO_3^- and NaF^- compounds formed in the CEI layer for the one-cycle electrodes (i. e., NFMO-w/o additives, NFMO-NC, and NFMO-NF). Optical images showing the morphological change of the surface during the TOF-SIMS analysis are additionally provided in Fig. S5. CO_3^- and NaF^- are chosen for tracking the Na_2CO_3 and NaF compounds because they are key products that determine the properties of the CEI layer on the NFMO electrode surface, as discussed in Figs. 3 and 4. Additionally, to define the depth of the CEI layer (i.e., the interface between the CEI layer and electrode surface), the TOF-SIMS spectra for transition metal species (FeO_2^- and MnO_2^-) were analyzed (Fig. S6). In Fig. 5a, the TOF-SIMS spectra of CO_3^- species for NFMO-NC and NFMO-NF (red and green lines, respectively) clearly demonstrate that they have higher contents of CO_3^- compared to NFMO-w/o additives (black line) at the very outer side of the CEI film (i.e., near the zero sputter time in the dotted box). Moreover, the depth profiles of NaF^- (Fig. 5b) demonstrate that NaF are deeply composed in the CEI layers of NFMO-NC and NFMO-NF compared to the NFMO-w/o additives. In other words, relatively thicker CEI layers were formed on NFMO-NC and NFMO-NF, and their outside surface is mostly composed of CO_3^- carbonates. The depth profiles of CO_3^- and NaF^- verify that the use of additives can change the thickness of CEI layer as well as induce compositional changes. To further check a CEI thickness affected by the additive, energy-dispersive X-ray spectroscopy (EDS) line-scanning profiles by using transmission electron microscopy (TEM) were analyzed and discussed in Fig. S7. In short, our XAS, XPS, TOF-SIMS, and TEM analyses clearly prove that the addition of Na_2CO_3 and NaF into the electrolyte is effective way to
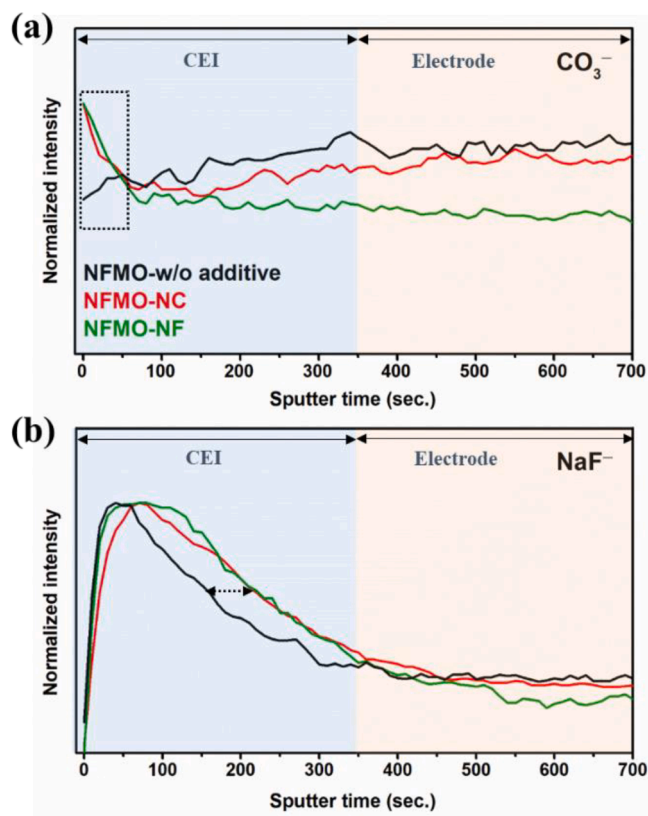

Fig. 5. TOF-SIMS depth profiles of inorganic secondary ion fragments (normalized to the maximum) on the surfaces of the one-cycle NFMO electrodes (NFMO-w/o additives, NFMO-NC, and NFMO-NF). The TOF-SIMS depth profiles show the evolution of the (a) CO_3^- and (b) NaF^- species in the CEI layer formed on the electrode surfaces.

modify CEI layer of NFMO to be mainly composed of robust Na_2CO_3 and NaF, which also serve to produce a thick and stable CEI layer. As a result, the newly formed CEI layer could improve electrochemical performances such as reversible capacities and cyclability by suppressing undesirable reactions at the NFMO surface.

3. Conclusions

In conclusion, to artificially form a stable and thick CEI layer on a high-voltage cathode material of NFMO, we used Na_2CO_3 (NFMO-NC) and NaF (NFMO-NF) as functional additives, and their effects were closely investigated. A key to achieve a stable NIB cathode with a long cycling life is providing high contents of Na_2CO_3 and NaF as major components of the CEI layer; therefore, we directly added these functional additives into the electrolyte and electrochemically decomposed them during the first charge process. It was demonstrated that comparatively thick CEI layers could be formed directly on the NFMO-NC and NFMO-NF surfaces, and they effectively improved the mechanical strength of the CEI layer. The high contents of Na_2CO_3 and NaF in the thick CEI layer were demonstrated by using XAS, XPS, and TOF-SIMS analyses. Additionally, we demonstrated that the thick CEI layer was effective for preventing the dissolution of active material, thereby leading to improved cycling stability. Consequently, the NFMO-NC and NFMO-NF electrodes could deliver high capacity retentions of 36.8 and 33.6%, respectively, after 500 cycles, while the bare NFMO electrode without additives only showed a capacity retention of 18.6%. The simple and effective approach to prevent the side reactions of high-voltage cathode materials will open new strategies for developing advanced NIBs.

4. Experimental section

4.1. Synthesis

NFMO was synthesized by using the solid-state method. Na_2CO_3, Mn_2O_3 and Fe_2O_3 were stoichiometrically mixed using wet ball milling in ethanol. The mixture was ball milled at 300 rpm for 20 min and dried to compress the sample into a pellet. The pellet was calcined in a box furnace at a temperature of 900°C for 12 h.

4.2. Electrochemistry

The prepared NFMO cathode material (AM) was mixed with carbon black (CB) and a PVDF binder at a ratio of AM: CB: PVDF = 75:15:10. N-Methyl-2-pyrrolidone (NMP) was used as a solvent for the preparation of the electrode slurry. Then, it was coated on aluminum foil and dried in a vacuum oven at 120°C for 4 h to remove residual solvent. Metallic sodium was used as a counter electrode, and conventional electrolytes of 1 M $NaClO_4$ in PC: FEC (98:2 by wt.%) with and without the 2 wt% Na_2CO_3 and NaF additives were used for the half-cell tests. All the electrochemical properties were tested by using a multichannel battery tester (Maccor version 4000), and the cutoff voltage was 1.5–4.3 V.

4.3. Material characterizatiom

For the *ex-situ* analysis, each NFMO sample was washed in dimethyl carbonate (DMC) and dried in an argon-filled glove box. An Rigaku Dmax 2500, X-ray diffractometer was used to obtain the X-ray diffraction (XRD) patterns. A Biologic potentiostat/galvanostat model VMP3 (BioLab, Inc.) was used for conducting the CV and EIS tests at a scan rate of 0.1 mV s^{-1}. To observe the chemical composition of the CEI layers on the surface of the electrodes, a PHI 5000 Versa Probe (Ulvac-PHI) equipped with a monochromator of Al–Kα (1486.6 eV) was used. The core-level spectra were energy-calibrated based on the adventitious C 1 s core-level peak at a binding energy of 284.6 eV. XAS was performed with the 10D KIST-PAL bending magnet beamline at the Pohang Light

Source (PAL). All the spectra were collected in total electron yield mode. An ION TOF (Münster) was used for the TOF-SIMS studies. The analysis chamber was maintained at ultrahigh vacuum with a pressure below 2×10^{-9} mbar. All detected secondary ions of interest possessed negative polarity. A pulsed 30 keV Bi_1^+ (9 ns)-ion beam set in spectrometry mode was applied for spectrum and depth profiling. A 500 eV Cs^+-ion beam was used for sputtering the cycled electrodes with a typical sputtered area of 400×400 μm. To observe the thickness of CEI layer on the electrodes, TEM (Talos F 200X, FEI) was used.

Declaration of Competing Interest

The authors declare that they have no known competing financial interests or personal relationships that could have appeared to influence the work reported in this paper.

Appendix A. Supplementary data

Supplementary data to this article can be found online at https://doi.org/10.1016/j.cej.2021.130547.

References

[1] J. Liu, J.-G. Zhang, Z. Yang, J.P. Lemmon, C. Imhoff, G.L. Graff, L. Li, J. Hu, C. Wang, J. Xiao, G. Xia, V.V. Viswanathan, S. Baskaran, V. Sprenkle, X. Li, Y. Shao, B. Schwenzer, Materials science and materials chemistry for large scale electrochemical energy storage: From transportation to electrical grid, Adv. Funct. Mater. 23 (8) (2013) 929–946.
[2] M.S. Islam, C.A.J. Fisher, Lithium and sodium battery cathode materials: Computational insights into voltage, diffusion and nanostructural properties, Chem. Soc. Rev. 43 (2014) 185–204.
[3] J.B. Goodenough, Rechargeable batteries: Challenges old and new, J. Solid State Electrochem. 16 (2012) 2019–2029.
[4] S. Paul, Materials and electrochemistry: Present and future battery, J. Electrochem. Sci. Technol. 7 (2016) 115–131.
[5] K. Kubota, S. Komaba, Review-practical issues and future perspective for Na-ion batteries, J. Electrochem. Soc. 162 (2015) A2538–A2550.
[6] J.Y. Hwang, S.T. Myung, Y.K. Sun, Sodium-ion batteries: Present and future, Chem. Soc. Rev. 46 (2017) 3529–3614.
[7] K.M. Abraham, Prospects and limits of energy storage in batteries, J. Phys. Chem. Lett. 6 (2015) 830–844.
[8] T. Liu, Y. Zhang, Z. Jiang, X. Zeng, J. Ji, Z. Li, X. Gao, M. Sun, Z. Lin, M. Ling, J. Zheng, C. Liang, Exploring competitive features of stationary sodium ion batteries for electrochemical energy storage, Energy Environ. Sci. 12 (2019) 1512–1533.
[9] J. Li, S.L. Glazier, J. Paulsen, J.R. Dahn, X. Ma, J. Harlow, Effect of Choices of Positive Electrode Material Electrolyte, Upper Cut-Off Voltage and Testing Temperature on the Life Time of Lithium-Ion Cells 165 (2018) 3195–3204.
[10] Y. Li, Y. Lu, C. Zhao, Y.S. Hu, M.M. Titirici, H. Li, X. Huang, L. Chen, Recent advances of electrode materials for low-cost sodium-ion batteries towards practical application for grid energy storage, Energy Storage Mater. 7 (2017) 130–151.
[11] C. Fang, Y. Huang, W. Zhang, J. Han, Z. Deng, Y. Cao, H. Yang, Routes to High Energy Cathodes of Sodium-Ion Batteries, Adv. Energy Mater. 6 (2016) 1501727.
[12] N. Yabuuchi, M. Kajiyama, J. Iwatate, H. Nishikawa, S. Hitomi, R. Okuyama, R. Usui, Y. Yamada, S. Komaba, P2-type Nax[Fe1/2Mn1/2]O2 made from earth-abundant elements for rechargeable NaÅ batteries, Nat. Mater. 11 (2012) 512–517.
[13] R.J. Clément, P.G. Bruce, C.P. Grey, Review—Manganese-Based P2-Type Transition Metal Oxides as Sodium-Ion Battery Cathode Materials, J. Electrochem. Soc. 14 (2015) 2589–2604.
[14] K. Zhang, D. Kim, Z. Hu, M. Park, G. Noh, Y. Yang, J. Zhang, V.W. hei Lau, S. L. Chou, M. Cho, S.Y. Choi, Y.M. Kang, Manganese based layered oxides with modulated electronic and thermodynamic properties for sodium ion batteries, Nat. Commun. 10 (2019) 520301–520312.
[15] G. Singh, J.M. López Del Amo, M. Galceran, S. Pérez-Villar, T. Rojo, Structural evolution during sodium deintercalation/intercalation in Na2/3[Fe1/2Mn1/2]O2, J. Mater. Chem. A. 3 (2015) 6954–6961.
[16] B. Mortemard De Boisse, D. Carlier, M. Guignard, L. Bourgeois, C. Delmas, P2-NaxMn1/2Fe1/2O2 phase used as positive electrode in Na batteries: Structural changes induced by the electrochemical (De)intercalation process, Inorg. Chem. 11197–11205 (2014).

[17] V. Duffort, E. Talaie, R. Black, L.F. Nazar, Uptake of CO 2 in Layered P2-Na 0.67 Mn 0.5 Fe 0.5 O 2: Insertion of Carbonate Anions, Chem. Mater. 27 (2015) 2515–2524.

[18] D. Susanto, M.K. Cho, G. Ali, J.Y. Kim, H.J. Chang, H.S. Kim, K.W. Nam, K. Y. Chung, Anionic Redox Activity as a Key Factor in the Performance Degradation of NaFeO2 Cathodes for Sodium Ion Batteries, Chem. Mater. 31 (2019) 3644–3651.

[19] S. Guo, Q. Li, P. Liu, M. Chen, H. Zhou, Environmentally stable interface of layered oxide cathodes for sodium-ion batteries, Nat. Commun. 8 (2017) 1–9.

[20] W. Yang, T.P. Devereaux, Anionic and cationic redox and interfaces in batteries: Advances from soft X-ray absorption spectroscopy to resonant inelastic scattering, J. Power Sources. 389 (2018) 188–197.

[21] W. Li, A. Dolocan, P. Oh, H. Celio, S. Park, J. Cho, A. Manthiram, Dynamic behaviour of interphases and its implication on high-energy-density cathode materials in lithium-ion batteries, Nat. Commun. 8 (2017) 14589.

[22] S. Liu, L. Wang, C. Zhang, B. Chu, C. Wang, T. Huang, A. Yu, Dynamic evolution of Cathode−Electrolyte interface of LiNi0.6Co0.2Mn0.2O2 during the initial Charge−Discharge process, J. Power Sources. 438 (2019).

[23] M.P. Do, N. Bucher, A. Nagasubramanian, I. Markovits, T. Bingbing, P.J. Fischer, K. P. Loh, F.E. Kühn, M. Srinivasan, Effect of Conducting Salts in Ionic Liquid Electrolytes for Enhanced Cyclability of Sodium-Ion Batteries, ACS Appl. Mater. Interfaces. 11 (2019) 23972–23981.

[24] Y. Okuno, K. Ushirogata, K. Sodeyama, Y. Tateyama, Decomposition of the fluoroethylene carbonate additive and the glue effect of lithium fluoride products for the solid electrolyte interphase: An ab initio study, Chem. Chem. Phys. 18 (2016) 8643–8653.

[25] K. Schroder, J. Alvarado, T.A. Yersak, J. Li, N. Dudney, L.J. Webb, Y.S. Meng, K. J. Stevenson, The Effect of Fluoroethylene Carbonate as an Additive on the Solid Electrolyte Interphase on Silicon Lithium-Ion Electrodes, Chem. Mater. 27 (2015) 5531–5542.

[26] V. Etacheri, O. Haik, Y. Goffer, G.A. Roberts, I.C. Stefan, R. Fasching, D. Aurbach, Effect of fluoroethylene carbonate (FEC) on the performance and surface chemistry of Si-nanowire li-ion battery anodes, Langmuir 28 (2012) 965–976.

[27] J. Kim, N. Go, H. Kang, A. Tron, J. Mun, Effect of fluoroethylene carbonate in the electrolyte for Lini0.5Mn1.5O4 cathode in lithium-ion batteries, J. Electrochem Sci. Technol. 8 (2017) 53–60.

[28] H.J. Song, S.H. Jang, J. Ahn, S.H. Oh, T. Yim, Artificial cathode-electrolyte interphases on nickel-rich cathode materials modified by silyl functional group, J. Power Sources. 416 (2019) 1–8.

[29] S.H. Jang, K.J. Lee, J. Mun, Y.K. Han, T. Yim, Chemically-induced cathode–electrolyte interphase created by lithium salt coating on Nickel-rich layered oxides cathode, J. Power Sources. 410–411 (2019) 15–24.

[30] H. Shin, J. Park, A.M. Sastry, W. Lu, Effects of fluoroethylene carbonate (FEC) on anode and cathode interfaces at elevated temperatures, J. Electrochem. Soc. 162 (2015) 9.

[31] J. Zheng, M.H. Engelhard, D. Mei, S. Jiao, B.J. Polzin, J.G. Zhang, W. Xu, Electrolyte additive enabled fast charging and stable cycling lithium metal batteries, Nat. Energy 2 (2017) 3.

[32] Y. Huang, L. Zhao, L. Li, M. Xie, F. Wu, R. Chen, Electrolytes and Electrolyte/ Electrode Interfaces in Sodium-Ion Batteries: From Scientific Research to Practical Application, Adv. Mater. 31 (2019) 1–41.

[33] G.G. Eshetu, T. Diemant, M. Hekmatfar, S. Grugeon, R.J. Behm, S. Laruelle, M. Armand, S. Passerini, Impact of the electrolyte salt anion on the solid electrolyte interphase formation in sodium ion batteries, Nano Energy 55 (2019) 327–340.

[34] R. Wang, X. Li, Z. Wang, H. Guo, T. Hou, G. Yan, B. Huang, Lithium carbonate as an electrolyte additive for enhancing the high-temperature performance of lithium manganese oxide spinel cathode, J. Alloys Compd. 618 (2015) 349–356.

[35] X. Cheng, J. Zheng, J. Lu, Y. Li, P. Yan, Y. Zhang, Realizing superior cycling stability of Ni-Rich layered cathode by combination of grain boundary engineering and surface coating, Nano Energy 62 (2019) 30–37.

[36] S. Komaba, W. Murata, T. Ishikawa, N. Yabuuchi, T. Ozeki, T. Nakayama, A. Ogata, K. Gotoh, K. Fujiwara, Electrochemical Na insertion and solid electrolyte interphase for hard-carbon electrodes and application to Na-ion batteries, Adv. Funct. Mater. 21 (2011) 3859–3867.

[37] J. Song, B. Xiao, Y. Lin, K. Xu, X. Li, Interphases in Sodium-Ion Batteries, Adv. Energy Mater. 8 (2018) 1703082.

[38] S. Doubaji, B. Philippe, I. Saadoune, M. Gorgoi, T. Gustafsson, A. Solhy, M. Valvo, H. Rensmo, K. Edström, Passivation Layer and Cathodic Redox Reactions in Sodium-Ion Batteries Probed by HAXPES, ChemSusChem 9 (2016) 97–108.

[39] N. Yabuuchi, M. Kajiyama, J. Iwatate, H. Nishikawa, S. Hitomi, R. Okuyama, R. Usui, Y. Yamada, S. Komaba, P2-type Nax [Fe1/2 Mn1/2]O2 made from earth-abundant elements for rechargeable NaÂ batteries, Nat. Mater. 11 (2012) 512–517.

[40] M. Sathiya, J. Thomas, D. Batuk, V. Pimenta, R. Gopalan, J.M. Tarascon, Dual Stabilization and Sacrificial Effect of Na2CO3 for Increasing Capacities of Na-Ion Cells Based on P2-NaxMO2 Electrodes, Chem. Mater. 29 (2017) 5948–5956.

[41] K.J. Park, J.Y. Hwang, H.H. Ryu, F. Maglia, S.J. Kim, P. Lamp, C.S. Yoon, Y.K. Sun, Degradation Mechanism of Ni-Enriched NCA Cathode for Lithium Batteries: Are Microcracks Really Critical? ACS Energy Lett. 4 (2019) 1394–1400.

[42] T. Li, X. Zi, Y. Lei, Z. Datong, S. Kaiyuan, S. Christina, Degradation Mechanisms and Mitigation Strategies of Nickel – Rich NMC – Based Lithium – Ion Batteries, Springer Singapore 3 (2019) 43–80.

[43] S.J. Rezvani, F. Nobili, R. Gunnella, M. Ali, R. Tossici, S. Passerini, A. Di Cicco, SEI Dynamics in Metal Oxide Conversion Electrodes of Li-Ion Batteries, J. Phys. Chem. C. 121 (2017) 26379–26388.

[44] A. Di Cicco, A. Giglia, R. Gunnella, S.L. Koch, F. Mueller, F. Nobili, M. Pasqualini, S. Passerini, R. Tossici, A. Witkowska, SEI Growth and Depth Profiling on ZFO Electrodes by Soft X-Ray Absorption Spectroscopy, Adv. Energy Mater. 5 (2015) 1500642.

[45] S.M. Bak, R. Qiao, W. Yang, S. Lee, X. Yu, B. Anasori, H. Lee, Y. Gogotsi, X.Q. Yang, Na-Ion Intercalation and Charge Storage Mechanism in 2D Vanadium Carbide, Adv. Energy Mater. 7 (2017) 20.

[46] T. Hou, G. Yang, N.N. Rajput, J. Self, S.W. Park, J. Nanda, K.A. Persson, The influence of FEC on the solvation structure and reduction reaction of LiPF6/EC electrolytes and its implication for solid electrolyte interphase formation, Nano Energy 64 (2019).